


# Twin Metamaterials: Inversion Symmetry, Reverse Magnetism, and Interface States

Xiaodong Sun,<sup>1</sup> Xinyu Zhao,<sup>1</sup> Jingguang Chen,<sup>2,3</sup> Fang Guan,<sup>2,3</sup> and Xinhua Hu<sup>1,\*</sup>

<sup>1</sup>*Department of Materials Science and Key Laboratory of Micro- and Nano-Photonic Structures (Ministry of Education), Fudan University, Shanghai 200433, China*

<sup>2</sup>*State Key Laboratory of Surface Physics, Institute for Nanoelectronic Devices and Quantum Computing, Fudan University, Shanghai 200433, China*

<sup>3</sup>*Zhangjiang Fudan International Innovation Center, Fudan University, Shanghai 201210, China*

 (Received 22 February 2023; revised 17 April 2023; accepted 3 May 2023; published 24 May 2023)

Artificial magnetism can be realized with metamaterials in high frequencies, which are important for many applications. However, such metamaterials need to be constructed with metal or high-relative-permittivity dielectric and thus may exhibit absorption loss. Here, we theoretically propose and experimentally demonstrate a pair of magnetic metamaterials that have inversion symmetry and are generated from a parent photonic crystal with low-relative-permittivity dielectric ( $\epsilon_r < 4$ ). Interestingly, one metamaterial is paramagnetic, the other is diamagnetic, and the product of their effective relative permeabilities is close to 1 ( $\mu_{e1} > 1$ ,  $\mu_{e2} < 1$ ,  $\mu_{e1}\mu_{e2} \approx 1$ ) in a broad frequency range. As a result, fascinating effects, such as wide-angle and wide-frequency near-perfect transmission and interface states, are observed in the systems.

DOI: [10.1103/PhysRevApplied.19.054081](https://doi.org/10.1103/PhysRevApplied.19.054081)

## I. INTRODUCTION

Magnetism is a fundamental property of materials, which is important for many applications [1,2]. Common materials can exhibit a strong electric response, whereas their magnetic response is usually very weak, with relative magnetic permeability  $\mu_r$  close to 1 ( $|\mu_r - 1| < 10^{-3}$ ). Ferromagnetic and antiferromagnetic materials can exhibit a strong magnetic response, but usually work in the frequency range below 2 THz [3–5]. For frequencies above 2 THz, all conventional materials will be nonmagnetic ( $\mu_r = 1$ ) [2,5,6].

In recent years, metamaterials have attracted great attention due to their unique ability for controlling electromagnetic (EM) waves [7–27]. Unlike conventional materials, metamaterials are composed of subwavelength building blocks or meta-atoms, which can be described by effective relative permittivity  $\epsilon_e$  and effective relative permeability  $\mu_e$ . By optimizing constituent materials and geometric parameters of such building blocks, metamaterials can possess extreme values of effective parameters, greatly broadening the range of EM parameters of materials [7–11]. For instance, using building blocks supporting magnetic resonance [7–15], metamaterials can be constructed that can exhibit a magnetic response for frequencies above 2 THz [9,11,15]. However, such magnetic metamaterials

are usually made of metal or dielectric with high relative permittivity [ $\text{Re}(\epsilon_r) > 10$ ], and thus may suffer from absorption loss.

In this paper, we theoretically propose and experimentally demonstrate a pair of magnetic metamaterials that are constructed with materials of low relative permittivity ( $\epsilon_r < 4$ ) and can exhibit a magnetic response in a broad frequency range. Here, the two metamaterials are generated from the same photonic crystal (PC) and thus are called twin metamaterials. Interestingly, one of the metamaterials is paramagnetic ( $\mu_{e1} > 1$ ), the other is diamagnetic ( $\mu_{e2} < 1$ ), and the product of their relative permeabilities is close to 1 ( $\mu_{e1}\mu_{e2} \approx 1$ ). As a result, fascinating phenomena, such as wide-angle and wide-frequency near-perfect transmission and interface states, are observed in such metamaterials.

## II. RESULTS

We first consider a one-dimensional (1D) layered PC, which is invariant in the  $y$ - $z$  plane, but periodic along the  $x$  direction, as shown in Fig. 1(a). The unit cell of the PC consists of four dielectric layers, where layer  $j$  ( $j = 1, 2, 3, 4$ ) has a thickness  $d_j$ , relative permittivity  $\epsilon_j$ , relative permeability  $\mu_j = 1$ , relative impedance  $Z_j = \sqrt{\mu_j}/\sqrt{\epsilon_j}$ , and refractive index  $n_j = \sqrt{\mu_j}\sqrt{\epsilon_j}$ . Light is assumed to propagate in the  $x$  direction with electric (magnetic) field in the  $y$  ( $z$ ) direction. The EM field in layer  $j$  can be written as  $E_y = E_j^+ p + E_j^- / p$  and  $H'_z =$

\*huxh@fudan.edu.cn

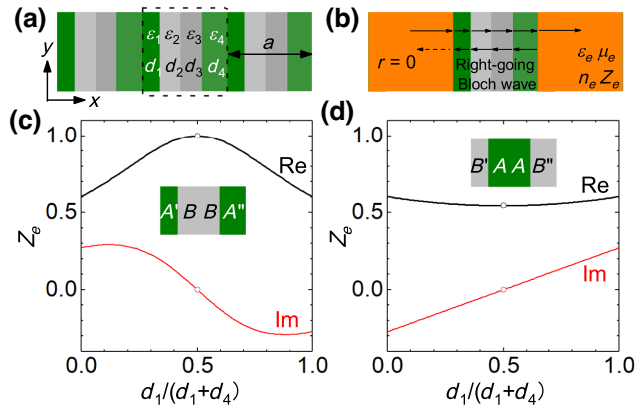


FIG. 1. (a) Schematic of a 1D layered PC, which is periodic in the  $x$  direction and has four dielectric layers in the unit cell. Here, layer  $j$  ( $j = 1, 2, 3, 4$ ) has a relative electric permittivity  $\epsilon_j$  and thickness  $d_j$ , and the lattice constant  $a = d_1 + d_2 + d_3 + d_4$ . (b) A unit cell is placed in an effective medium with parameters of  $\epsilon_e, \mu_e, n_e$ , and  $Z_e$ . (c) Real and imaginary parts of the effective relative impedance  $Z_e$  as a function of  $d_1$ . Here,  $\epsilon_1 = \epsilon_4 = 2.4, \epsilon_2 = \epsilon_3 = 1, d_2 = d_3 = 0.22a$ , and frequency  $f = 0.277c/a$ . (d) The same as (c) but for  $\epsilon_1 = \epsilon_4 = 1, \epsilon_2 = \epsilon_3 = 2.4$ , and  $d_2 = d_3 = 0.28a$ .

$E_j^+ p / Z_j - E_j^- / (p Z_j)$ , where the superscript  $+$  ( $-$ ) represents the right-going (left-going) wave,  $H'_z \equiv Z_0 H_z$ ,  $Z_0 = 376.73 \Omega$  is the impedance of vacuum,  $p = \exp[ik_j(x - x_j)]$ ,  $k_j = n_j k_0$ ,  $k_0 = \omega/c$  is the wave number in vacuum,  $\omega \equiv 2\pi f$  is angular frequency,  $f$  is frequency,  $c$  is the light speed in vacuum, and  $x = x_j$  ( $x_j + d_j$ ) at the left (right) surface of layer  $j$ . Hence, the fields are  $E_{j,L} = E_j^+ + E_j^-$  and  $H'_{j,L} = E_j^+ / Z_j - E_j^- / Z_j$  ( $E_{j,R} = E_j^+ p_j + E_j^- / p_j$  and  $H'_{j,R} = E_j^+ p_j / Z_j - E_j^- / (p_j Z_j)$  with  $p_j = \exp(ik_j d_j)$ ) at the left (right) surface of layer  $j$ . Using a characteristic matrix [28],

$$M_j = \begin{pmatrix} \cos(k_j d_j) & -i \sin(k_j d_j) Z_j \\ -i \sin(k_j d_j) / Z_j & \cos(k_j d_j) \end{pmatrix}, \quad (1)$$

the fields at the left surface of layer  $j$  can be related to those at its right surface:

$$\begin{pmatrix} E_{j,L} \\ H'_{j,L} \end{pmatrix} = M_j \begin{pmatrix} E_{j,R} \\ H'_{j,R} \end{pmatrix}. \quad (2)$$

Similarly, the fields at the left surface of the unit cell can be obtained from those at its right surface:

$$\begin{pmatrix} E_{1,L} \\ H'_{1,L} \end{pmatrix} = M \begin{pmatrix} E_{4,R} \\ H'_{4,R} \end{pmatrix}, \quad (3)$$

where the characteristic matrix of the unit cell is given by

$$M = M_1 M_2 M_3 M_4 = \begin{pmatrix} m_{11} & m_{12} \\ m_{21} & m_{22} \end{pmatrix}, \quad (4)$$

with  $m_{11}$  and  $m_{22}$  being real and  $m_{12}$  and  $m_{21}$  being pure imaginary.

The Bloch theorem can then be applied to the unit cell:

$$M \begin{pmatrix} E_{4,R} \\ H'_{4,R} \end{pmatrix} = g \begin{pmatrix} E_{4,R} \\ H'_{4,R} \end{pmatrix}, \quad (5)$$

where  $g = \exp(-iqa)$ ,  $q$  is the Bloch wave number, and  $a = d_1 + d_2 + d_3 + d_4$  is the lattice constant. Hence, we have

$$g = \left[ m_{11} + m_{22} \pm \sqrt{(m_{11} - m_{22})^2 + 4m_{12}m_{21}} \right] / 2, \quad (6)$$

so that the Bloch wave number  $q = i \ln(g) / a$  and effective refractive index  $n_e \equiv q/k_0$  can be calculated. Here, the plus or minus sign in Eq. (6) can be determined by choosing the right-going Bloch wave with  $\text{Re}(q) > 0$  and  $\text{Im}(q) \geq 0$ .

To obtain the effective relative impedance  $Z_e$  of the PC, we consider a unit cell that is placed in its effective medium, as shown in Fig. 1(b). An EM plane wave is incident upon the unit cell from the left, with electric (magnetic) field in the  $y$  ( $z$ ) direction. Since the effective medium is equivalent to the unit cell, no reflected waves exist on the left, and only the right-going Bloch wave occurs in the unit cell. Using Eq. (5) and  $Z_e = E_{4,R}/H'_{4,R}$ , we have

$$Z_e = (g - m_{22}) / m_{21}. \quad (7)$$

We note that Eq. (6) can also be derived by using  $(E_i, E_i/Z_e)^T = M (E_i, E_i/Z_e)^T$ , where  $E_i$  ( $E_i$ ) is the  $E$ -field of the incident (transmitted) wave at the left (right) surface of the unit cell. The effective relative permittivity  $\epsilon_e = n_e/Z_e$  and effective relative permeability  $\mu_e = n_e Z_e$  can thus be calculated for the PC.

When the unit cell does not have inversion symmetry (so that  $m_{11} \neq m_{22}$ ), the relative impedance  $Z_e$  depends on the direction of the incident wave:

$$Z_{e,L} = Z_{e,R}^*, \quad (8)$$

where  $Z_{e,L}$  ( $Z_{e,R}$ ) is the relative impedance of the PC for a wave incident from the left (right).  $Z_{e,L}$  and  $Z_{e,R}$  are complex even in the passing band. When an asymmetric PC is placed in air, its left and right surfaces will exhibit the same intensities  $|r|^2$  but different phases  $\arg(r)$  in reflection [ $r = (Z_e - 1)/(Z_e + 1)$ ]. However, if the unit cell has inversion symmetry (so that  $m_{11} = m_{22}$ ), the same relative impedance can be obtained for incident waves from different directions ( $Z_e = Z_{e,L} = Z_{e,R}$ ). The relative impedance  $Z_e$  is real in the passing band and pure imaginary in the band gaps.

Using a parent layered PC  $(AABB)_n$ , two PCs with inversion symmetry,  $(ABBA)_n$  and  $(BAAB)_n$  (called PC1 and

PC2), can be generated. Such twin PCs can have the same effective refractive index ( $n_{e1} = n_{e2}$ ) but different relative impedance ( $Z_{e1} \neq Z_{e2}$ ). It can be proved that for the lowest band and the first band gap,  $\sqrt{Z_{e1}Z_{e2}} \approx Z_{e0} = 1/n_{e0}$ , where  $Z_{e0}$  ( $n_{e0} = \sqrt{a^{-1} \sum_{j=1}^4 \varepsilon_j d_j}$ ) is  $Z_e$  ( $n_e$ ) at zero frequency. In the lowest band,  $n_{e1} = n_{e2} \approx n_{e0}$  and  $\mu_{e1}\mu_{e2} \approx 1$ . When the relative permittivity of layer  $A$  is higher than that of layer  $B$  ( $\varepsilon_A > \varepsilon_B$ ), PC1 and PC2 will be paramagnetic ( $\mu_{e1} > 1$ ) and diamagnetic ( $\mu_{e2} < 1$ ), respectively. Although a slight dependence of the relative impedance on the termination of the unit cell has been noticed [29], the reverse magnetism of PC1 and PC2 has not been discovered in previous studies.

Based on the above theory, we investigate a 1D layered PC  $(AABB)_n$ , where layer  $A$  ( $B$ ) has a relative permittivity  $\varepsilon_A = 2.4$  ( $\varepsilon_B = 1$ ) and thickness  $d_A = 0.28a$  ( $d_B = 0.22a$ ). Such materials with low relative permittivity ( $\varepsilon_r < 4$ ) can be achieved in various frequency ranges. For example, glass has a relative permittivity of 2.13 in optical frequencies [30]. Using this parent PC, two kinds of daughter PCs,  $(A'BBA'')_n$  and  $(B'AAB'')_n$  (called PC1' and PC2'), can be generated. Here, layers  $A'$  and  $A''$  ( $B'$  and  $B''$ ) have a relative permittivity of  $\varepsilon_A$  ( $\varepsilon_B$ ) and total thickness  $d_1 + d_4 = 2d_A$  ( $d_1 + d_4 = 2d_B$ ). When  $d_1 = d_4$ , PC1' (PC2') will become PC1 (PC2).

Figure 1(c) shows the relative impedance of PC1' as a function of the thickness  $d_1$  of layer  $A'$  at frequency  $f = 0.277c/a$ . The relative impedances of  $(CAAD)_n$  and  $(DAAC)_n$  are found to be conjugate [Eq. (8)], showing that an asymmetric PC has the same intensities but different phases in reflection for incident waves from different directions. When the unit cell has inversion symmetry ( $d_1 = d_4$ ),  $Z_e$  will be real ( $Z_e = 1$ ). Similar results are also found for PC2', as shown in Fig. 1(d). When  $d_1 = d_4$ ,  $Z_e$  will also be real, but with a different value ( $Z_e = 0.544$ ). This means that a symmetric PC has the same reflection coefficients for incident waves from different directions.

We then focus on the twin PCs with inversion symmetry, PC1 and PC2, as shown in Figs. 2(a) and 2(b). Since they originate from the same parent PC, the twin PCs have the same effective refractive index  $n_e$  [see Fig. 2(b)]. Here,  $n_e$  is 1.335 at  $f = 0$  and increases slightly with increasing the frequency, with a relative change less than 10% in the lowest band. Figure 2(c) shows the relative impedance  $Z_{e1}$  ( $Z_{e2}$ ) of PC1 (PC2) as a function of frequency. We can see that PC1 and PC2 have the same effective relative impedance ( $Z_{e1} = Z_{e2} = 0.749$ ) at  $f = 0$ . As the frequency increases, the relative impedance  $Z_{e1}$  ( $Z_{e2}$ ) increases (decreases). However, their geometric mean  $\sqrt{Z_{e1}Z_{e2}}$  is nearly unchanged, with a relative change less than 2.5% in the first band. Therefore, for normally incident waves from air, the reflection of PC1 [ $R = |(Z_e - 1)/(Z_e + 1)|^2$ ] is lower than that of PC2, as

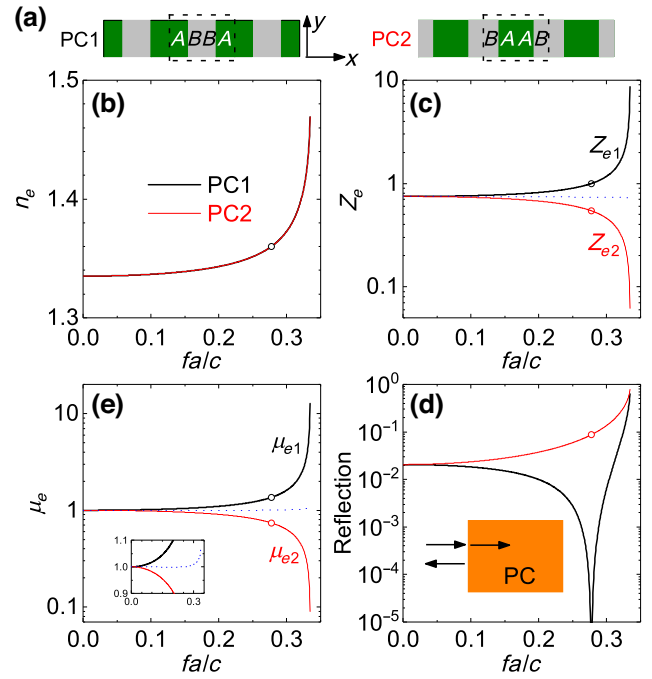


FIG. 2. (a) Schematic of twin metamaterials of PC1 and PC2  $[(ABBA)_n$  and  $(BAAB)_n$ ], where layer  $A$  ( $B$ ) has parameters of  $\varepsilon_A = 1$  and  $d_A = 0.22a$  ( $\varepsilon_B = 2.4$  and  $d_B = 0.28a$ ). (b) Effective refractive index  $n_e$ , (c) effective relative impedance  $Z_e$ , (d) reflection  $R$ , and (e) effective relative permeability  $\mu_e$  as a function of frequency  $f$ . In (d), light is normally impinging upon semi-infinite PC1 and PC2 that exist in the region of  $x > 0$ . The blue dashed lines in (c),(e) represent  $\sqrt{Z_{e1}Z_{e2}}$  and  $\sqrt{\mu_{e1}\mu_{e2}}$ , respectively.

shown in Fig. 3(d). At  $f = 0.277c/a$ , the reflection of PC1 and PC2 is 0 and 8.7%, respectively.

We note that the impedance  $Z_e$  is the ratio of the electric field  $E$  to the reduced magnetic field  $H'$ . For a given Bloch wave, the ratio of  $Z_e$  can be different at different positions in the unit cell. When the Bloch wave is a standing wave ( $|E_j^+| = |E_j^-|$ ),  $E$  or  $H'$  can be 0 at a certain location (i.e., node), corresponding to  $Z_e = 0$  or  $\infty$ . This is why PC1 and PC2 have different impedances. Such a difference in impedance reflects that the field of Bloch waves ( $E$  and  $H'$ ) has significant fluctuations in intensity, especially in high frequencies. However, the geometric mean of the surface impedance of PC1 and PC2 ( $\sqrt{Z_{e1}Z_{e2}}$ ) changes little with frequency, which is very close to the ratio of the average electric field  $E$  to the average magnetic field  $H'$  for the right-going Bloch wave.

Similar bifurcation behavior is also found in the effective permeabilities of PC1 and PC2, as shown in Fig. 2(e). At zero frequency, the twin PCs are nonmagnetic ( $\mu_{e1} = \mu_{e2} = 1$ ). With an increase of frequency, the relative permeability of PC1 increases ( $\mu_{e1} > 1$ ), while that of PC2 decreases ( $\mu_{e2} < 1$ ). At  $f = 0.277c/a$ , the twin PCs can

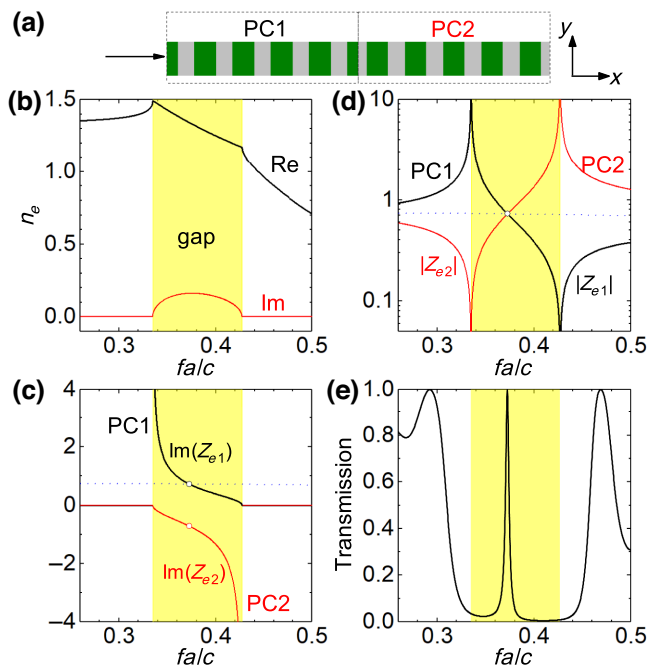


FIG. 3. (a) Schematic of a 1D layered structure  $(ABBA)_5(BAAB)_5$ , where the dielectric layers  $A$  and  $B$  have the same parameters as in Fig. 2. (b) Effective refractive index  $n_e$ , (c)  $\text{Im}(Z_e)$ , and (d)  $|Z_e|$  of PC1 and PC2 [ $(ABBA)_n$  and  $(BAAB)_n$ ] as a function of frequency  $f$ . (e) Transmission spectrum of the structure in (a) at normal incidence. The blue dashed lines in (c),(d) represent  $\sqrt{Z_{e1}Z_{e2}}$ . The yellow areas in (b)–(e) denote the lowest photonic band gap.

exhibit a magnetic response ( $\mu_{e1} = 1.36$  and  $\mu_{e2} = 0.74$ ) much stronger than that of conventional paramagnetic and antimagnetic materials ( $|\mu_r - 1| < 10^{-3}$ ). Interestingly, the product of the relative permeabilities of the twin PCs is close to 1 in the whole lowest band.

Figure 3 shows the properties of the twin PCs at the first band gap. Here, PC1 and PC2 have the same gap range ( $0.335 < fa/c < 0.427$ ) and same effective refractive index  $n_e$ .  $\text{Im}(n_e) > 0$  in the band gap, denoting evanescent Bloch waves [Fig. 3(b)]. Figures 3(c) and 3(d) show the relative impedance of the twin PCs. In the band gap, the relative impedance becomes a pure imaginary number  $bi$  with  $b > 0$  ( $b < 0$ ) for PC1 (PC2). At the lower gap edge ( $f = 0.335c/a$ ), PC1 (PC2) behaves like a perfect magnetic (electric) conductor, with  $|Z_{e1}| = |\mu_{e1}| = \infty$  ( $|Z_{e2}| = |1/\varepsilon_{e2}| = 0$ ). However, at the upper gap edge ( $f = 0.427c/a$ ), PC1 (PC2) is similar to a perfect electric (magnetic) conductor, with  $Z_{e1} = 0$  ( $|Z_{e2}| = \infty$ ). Interestingly, the geometric mean value of their relative impedances  $\sqrt{Z_{e1}Z_{e2}}$  is still nearly unchanged in the gap. At  $f = 0.373c/a$ , PC1 and PC2 have opposite relative impedance ( $Z_{e1} = -Z_{e2} = 0.725i$ ). Therefore, an interface state will appear at this frequency when PC1 and PC2 are connected together [31]. When light is normally incident

on a structure  $(ABBA)_5(BAAB)_5$ , complete transmission can be observed in the band gap, as shown in Fig. 3(e).

The above effects can also be realized in higher dimensions. Figure 4 shows an example in two dimensions (2D). Here, two PCs with inversion symmetry, called PC3 and PC4, are generated from a parent 2D PC, consisting of a square lattice of air cylinders in a dielectric background. Air (dielectric) is located at the center of the unit cell of PC3 (PC4). The air cylinders have a radius  $r = 0.375a$ , the dielectric has a relative permittivity of 2.4, and the lattice constant is  $a$ . By using a commercial software (COMSOL Multiphysics) with a finite-element method, we can obtain the frequency and field distribution for Bloch waves propagating in the  $+x$  direction in the twin PCs (with a given wave number  $q$ ). Here, the electric field is in the  $x$ - $y$  plane and the magnetic field is parallel to the cylinders (in the  $z$  direction). Using  $n_e = q/k_0$  and  $Z_e = E_{y,a}/H'_{z,a}$  with  $E_{y,a}$  ( $H'_{z,a}$ ) being the average value of  $E_{y,a}$  ( $H'_{z,a}$ ) along the left

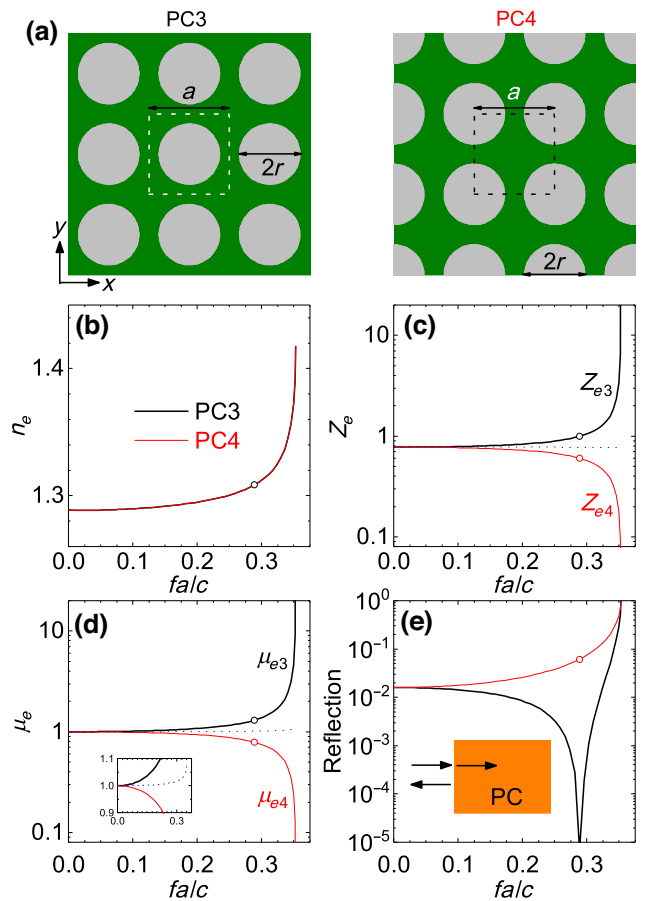


FIG. 4. (a) Schematic of twin metamaterials of PC3 and PC4, which are 2D PCs consisting of a square lattice of air cylinders in a dielectric medium. The dielectric has a relative permittivity of 2.4, the air cylinders have a radius  $r = 0.375a$ , and the lattice constant is  $a$ . (b)–(e) The same as Figs. 2(b)–2(e) but for PC3 and PC4. The blue dashed lines in (c),(e) represent  $\sqrt{Z_{e3}Z_{e4}}$  and  $\sqrt{\mu_{e3}\mu_{e4}}$ , respectively.

border of the unit cell, the effective parameters and reflection in the lowest band can thus be obtained, as shown in Figs. 4(b) and 4(c). When diffraction does not occur ( $fa/c < 1$ ), the reflection calculated from the effective parameters will be exactly the same as that from the real structure for a finite thickness of 2D PC in air (not shown). We can see that PC3 and PC4 have the same effective refractive index, but different values of relative impedance, reflection, and relative permeability. Here, PC3 is paramagnetic ( $\mu_{e3} > 1$ ), PC4 is diamagnetic ( $\mu_{e4} < 1$ ), and their relative permeabilities are nearly reciprocal to each other ( $\mu_{e3}\mu_{e4} \approx 1$ ). We note that in previous studies of metamaterials, the border of the unit cell cannot pass through scatterers and the scatterer is usually located at the center of the unit cell (similar to PC3). Since the case with air at the center of the unit cell (similar to PC4) has not been studied, the inverse magnetism of PC3 and PC4 has not been discovered in previous studies.

To verify the above theory, we perform microwave experiments on the twin PCs of PC1 and PC2. Four samples of  $ABBA$ ,  $BAAB$ ,  $(ABBA)_5$ , and  $(BAAB)_5$  are fabricated, where  $A$  is a layer of polytetrafluoroethylene glass fiber,  $B$  is an air layer, the lattice constant  $a = 2.72$  mm, and other parameters are the same as in Fig. 2. The sample is placed between a microwave source and a receiver [Figs. 5(a) and 5(b)]. Using a vector network analyzer (Keysight N5245B), the transmission spectra are measured for the samples at normal incidence, as shown in Figs. 5(c) and 5(d). We can see that the reflection of PC1 is lower

than that of PC2. PC1 can exhibit very low reflection at 30.62 GHz due to the impedance matching ( $Z_{e1} = 1$ ). This is different from common reflection dips [at  $f = ma/(2n_eL)$  with  $m$  being a positive integer] dependent on the thickness ( $L = na$ ) of the sample. Using a rotatable platform, the transmission spectra are also measured for the samples at oblique incidence of  $p$  waves (with magnetic field parallel to the surface of the sample) with  $f = 30.62$  GHz, as shown in Fig. 5(e). It is found that both PC1 and PC2 can show perfect transmission at the same incident angle of  $\theta_b = 57^\circ$ . Combining the Brewster angle and impedance matching effects, PC1 can exhibit high transmission in a wide range of incident angles [32]. Simulations are also performed with the transfer matrix method for realistic structures, as shown in Figs. 5(f)–5(h). Good agreement is found between the experiments and simulations. The difference between Figs. 5(d) and 5(g) may arise from the imperfection of the experimental samples.

We note that a field-averaging method has been proposed to understand the effective parameters of metamaterials [33]. For our 1D system, the formulas of the field-averaging method are  $n_e = c\sqrt{D_a B_a / (E_{4,R} H_{4,R})}$  and  $Z_e = \sqrt{E_{4,R} B_a / (H_{4,R} D_a)} / Z_0$  with  $B_a$  ( $D_a$ ) being the average value of  $B_z$  ( $D_y$ ) over the unit cell, which are different from our accurate formulas ( $n_e = q/k_0$  and  $Z_e = E_{4,R}/H_{4,R}$ ). In fact, our results cannot be understood quantitatively by the field-averaging method. Using the effective parameters from the field-averaging method, we calculate the transmission spectra for the above 1D PC samples

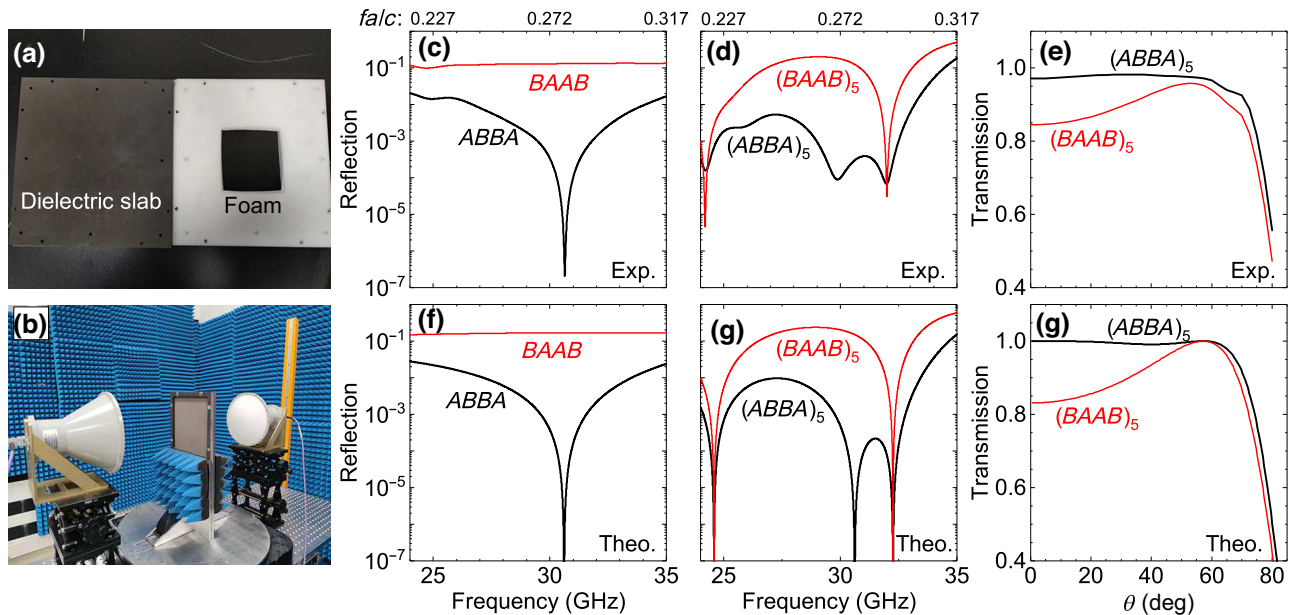


FIG. 5. (a) Photograph of an experimental sample. (b) Photograph of the experimental setup, where a sample is placed between a microwave source and receiver. (c),(f) Reflection spectra of samples  $ABBA$  and  $BAAB$  at normal incidence, where the lattice constant  $a = 2.72$  mm and other parameters are the same as in Fig. 2. (d),(g) The same as (c),(f) but for samples  $(ABBA)_5$  and  $(BAAB)_5$ . (e),(h) Transmission at 30.62 GHz as a function of incident angle for samples  $(ABBA)_5$  and  $(BAAB)_5$  under illumination of  $p$  waves. (c)–(e) Experimental results and (f)–(h) calculated results.

in air (not shown). It is found that when the scatterer is at the center of the unit cell (PC2), the field-averaging method can provide correct results only in low frequencies ( $fa/c < 0.1$ ). When air is at the center of the unit cell (PC1), the field-averaging method is valid only in lower frequencies ( $fa/c < 0.02$ ).

### III. SUMMARY

In summary, we demonstrate that based on an all-dielectric parent PC, twin metamaterials can be generated, which can possess inverse magnetism in a wide frequency range (i.e., the lowest band). Here, one metamaterial is paramagnetic ( $\mu_{e1} > 1$ ), the other is diamagnetic ( $\mu_{e2} < 1$ ), and the product of their effective relative permeabilities is close to 1 ( $\mu_{e1}\mu_{e2} \approx 1$ ). As a result, fascinating phenomena, such as wide-angle and wide-frequency near-perfect transmission and interface states, are observed in such metamaterials. Since the twin metamaterials only need to have inversion symmetry and can be constructed with low-relative-permittivity materials ( $\epsilon_r < 4$ ), they can be realized in high dimensions and in various frequency ranges including visible frequencies.

### ACKNOWLEDGMENTS

This work is supported by the National Key Research and Development Program of China (2018YFA0306201) and NSFC (61422504 and 11574037).

- 
- [1] K. M. Krishnan, *Fundamentals and Applications of Magnetic Materials* (Oxford University Press, Oxford, 2016).
- [2] L. D. Landau and E. M. Lifshitz, *Electrodynamics of Continuous Media* (Pergamon Press, Oxford, 1984).
- [3] P. Grunberg and F. Metawe, Light Scattering from Bulk and Surface Spin Waves in EuO, *Phys. Rev. Lett.* **39**, 1561 (1977).
- [4] L. Remer, B. Luthi, H. Sauer, R. Geick, and R. E. Camley, Nonreciprocal Optical Reflection of the Uniaxial Antiferromagnet MnF<sub>2</sub>, *Phys. Rev. Lett.* **56**, 2752 (1986).
- [5] T. J. Yen, W. J. Padilla, N. Fang, D. C. Vier, D. R. Smith, J. B. Pendry, D. N. Basov, and X. Zhang, Terahertz magnetic response from artificial materials, *Science* **303**, 1494 (2004).
- [6] R. Merlin, Metamaterials and the Landau–Lifshitz permeability argument: Large permittivity begets high-frequency magnetism, *Proc. Natl. Acad. Sci. U. S. A.* **106**, 1693 (2009).
- [7] J. B. Pendry, A. J. Holden, D. J. Robbins, and W. J. Stewart, Magnetism from conductors and enhanced nonlinear phenomena, *IEEE Trans. Microwave Theory Tech.* **47**, 2075 (1999).
- [8] R. A. Shelby, D. R. Smith, and S. Schultz, Experimental verification of a negative index of refraction, *Science* **292**, 77 (2001).
- [9] S. Linden, Christian Enkrich, Martin Wegener, Jiangfeng Zhou, Thomas Koschny, and Costas M. Soukoulis, Magnetic response of metamaterials at 100 terahertz, *Science* **306**, 1351 (2004).
- [10] J. Zhou, Th. Koschny, M. Kafesaki, E. N. Economou, J. B. Pendry, and C. M. Soukoulis, Saturation of the Magnetic Response of Split-Ring Resonators at Optical Frequencies, *Phys. Rev. Lett.* **95**, 223902 (2005).
- [11] V. M. Shalaev, Optical negative-index metamaterials, *Nat. Photon.* **1**, 41 (2007).
- [12] S. O’Brien and J. B. Pendry, Photonic band-gap effects and magnetic activity in dielectric composites, *J. Phys. Condens. Mater.* **14**, 4035 (2002).
- [13] B. I. Popa and S. A. Cummer, Compact Dielectric Particles as a Building Block for Low-Loss Magnetic Metamaterials, *Phys. Rev. Lett.* **100**, 207401 (2008).
- [14] Q. Zhao, J. Zhou, F. Zhang, and D. Lippens, Mie resonance-based dielectric metamaterials, *Mater. Today* **12**, 60 (2009).
- [15] L. Shi, T. U. Tuzer, R. Fenollosa, and F. Meseguer, A new dielectric metamaterial building block with a strong magnetic response in the sub-1.5-micrometer region: Silicon colloid nanocavities, *Adv. Mater.* **24**, 5934 (2012).
- [16] L. Feng, Ye-Long Xu, William S. Fegadolli, Ming-Hui Lu, José E. B. Oliveira, Vilson R. Almeida, Yan-Feng Chen, and Axel Scherer, Experimental demonstration of a unidirectional reflectionless parity-time metamaterial at optical frequencies, *Nature Mater.* **12**, 108 (2013).
- [17] P. Moitra, Yuanmu Yang, Zachary Anderson, Ivan I. Kravchenko, Dayrl P. Briggs, and Jason Valentine, Realization of an all-dielectric zero-index optical metamaterial, *Nat. Photon.* **7**, 791 (2013).
- [18] C. M. Watts, David Shrekenhamer, John Montoya, Guy Lipworth, John Hunt, Timothy Sleasman, Sanjay Krishna, David R. Smith, and Willie J. Padilla, Terahertz compressive imaging with metamaterial spatial light modulators, *Nature Photon.* **8**, 605 (2014).
- [19] S. Dai, Q. Ma, M. K. Liu, T. Andersen, Z. Fei, M. D. Goldflam, M. Wagner, K. Watanabe, T. Taniguchi, M. Thiemens, F. Keilmann, G. C. A. M. Janssen, S-E. Zhu, P. Jarillo-Herrero, M. M. Fogler, and D. N. Basov, Graphene on hexagonal boron nitride as a tunable hyperbolic metamaterial, *Nat. Nanotech.* **10**, 682 (2015).
- [20] S. Jahani and Z. Jacob, All-dielectric metamaterials, *Nature Nanotech.* **11**, 23 (2016).
- [21] J. P. Balthasar Mueller, N. A. Rubin, R. C. Devlin, B. Groever, and F. Capasso, Metasurface Polarization Optics: Independent Phase Control of Arbitrary Orthogonal States of Polarization, *Phys. Rev. Lett.* **118**, 113901 (2017).
- [22] H. Liu, Cheng Guo, Giulio Vampa, Jingyuan Linda Zhang, Tomas Sarmiento, Meng Xiao, Philip H. Bucksbaum, Jelena Vučković, Shanhui Fan, and David A. Reis, Enhanced high-harmonic generation from an all-dielectric metasurface, *Nat. Phys.* **14**, 1006 (2018).
- [23] K. Koshelev, S. Lepeshov, M. Liu, A. Bogdanov, and Y. Kivshar, Asymmetric Metasurfaces with High-Q Resonances Governed by Bound States in the Continuum, *Phys. Rev. Lett.* **121**, 193903 (2018).
- [24] M. Kadic, G. W. Milton, M. van Hecke, and M. Wegener, 3D metamaterials, *Nat. Rev. Phys.* **1**, 198 (2019).
- [25] H. Ren, Xinyuan Fang, Jaehyuck Jang, Johannes Bürger, Junsuk Rho, and Stefan A. Maier, Complex-amplitude

- metasurface-based orbital angular momentum holography in momentum space, *Nat. Nanotech.* **15**, 948 (2020).
- [26] A. H. Dorrah, Metasurface optics for on-demand polarization transformations along the optical path, *Nat. Photon.* **15**, 287 (2021).
- [27] W. J. Padilla and R. D. Averitt, Imaging with metamaterials, *Nature Rev. Phys.* **4**, 85 (2022).
- [28] M. Born and E. Wolf, *Principles of Optics* (Cambridge University Press, Cambridge, 2019), 7th ed.
- [29] D. R. Smith, D. C. Vier, Th. Koschny, and C. M. Soukoulis, Electromagnetic parameter retrieval from inhomogeneous metamaterials, *Phys. Rev. E* **71**, 036617 (2005).
- [30] E. D. Palik, *Handbook of Optical Constants of Solids*, (Academic Press, New York, 1985).
- [31] M. Xiao, Z. Q. Zhang, and C. T. Chan, Surface impedance and bulk band geometric phases in one-dimensional systems, *Phys. Rev. X* **4**, 021017 (2014).
- [32] K. Im, J. H. Kang, and Q. H. Park, Universal impedance matching and the perfect transmission of white light, *Nat. Photon.* **12**, 143 (2018).
- [33] D. R. Smith and J. B. Pendry, Homogenization of metamaterials by field averaging (invited paper), *J. Opt. Soc. Am. B* **23**, 391 (2006).